Improved Model Predictive Control With New Cost Function for Hybrid-Inverter Open-Winding PMSM System Based on Energy Storage Model

Chong Sun, Dan Sun, *Senior Member, IEEE*, Wenhan Chen, and Heng Nian, *Senior Member, IEEE*

***Abstract*—Conventional model predictive control (C-MPC) usually leads to considerable torque and current ripples since only one voltage vector is applied. In addition, the C-MPC applied in the hybrid-inverter) driven open-winding permanent magnet synchronous motor (OW-PMSM) suffers from complex tuning work of weighting factors and iterated evaluation work of all potential vectors because the capacitor voltage constraint in cost function is related to the switching states. In this article, an improved three-vector MPC based on energy storage model is proposed for the HI-OW-PMSM system. Firstly, a new prediction model of dc-link capacitor voltage based on energy storage model is proposed thus the capacitor voltage constraint is decoupled to the three-phase switching states. Furthermore, a novel restructured cost function without weighting factors can be obtained. Accordingly, by using the new prediction model and the novel cost function, the voltage reference can be easily obtained and a three-vector based prediction strategy without sector division can be carried out to achieve optimal voltage vectors selection and duty cycle calculation. Therefore, the system performance is improved and the calculation burden is also reduced. Finally, comparative experimental studies are carried out to validate the effectiveness of the proposed improved three-vector MPC method.**

***Index Terms*—Model predictive control (MPC), permanent magnet synchronous motor (PMSM), simplified three-vector selection strategy.**

I. Introduction

PERMANENT magnet synchronous motors (PMSMs) have been widely used in various motor drives, e.g., electric vehicle, aerospace and transportation due to their great advantages of simple structure, high power density and efficiency [1]–[3]. Meanwhile, open winding topology has gained popularity owing to its great features such as two terminal inputs/outputs, flexible power supply modes, multilevel characteristic and fault-tolerant capability [4]–[7]. Therefore, the open winding permanent magnet synchronous motor (OW-PMSM) system has drawn increasing attentions [8]–[10].

Manuscript received September 23, 2020; revised January 3, 2021; accepted February 10, 2021. Date of publication February 23, 2021; date of current version June 1, 2021. This work was supported by the National Natural Science Foundation of China under Grant 51877197. Recommended for publication by Associate Editor R. Kennel. *(Corresponding author: Dan Sun.)*

The authors are with the College of Electrical Engineering, Zhejiang University, Hangzhou 310027, China (e-mail: 21610050@zju.edu.cn; sundan@zju.edu.cn; sorachen@zju.edu.cn; nianheng@zju.edu.cn).

Color versions of one or more figures in this article are available at https://doi.org/10.1109/TPEL.2021.3061497.

Digital Object Identifier 10.1109/TPEL.2021.3061497

The OW-PMSM system can be characterized by different power supply topology, including common dc bus topology [8], isolated power supply topology [9] and hybrid power supply topology [10], [11]. Among these different kinds of topologies, the hybrid power supply topology applies a dc power source and a floating dc-link capacitor to supply the power of two isolated inverters and it is also called as hybrid-inverter (HI) structure [10], [11]. Compared with the other two kinds of structures, the HI structure requires only one power source and has no zero sequence circuit, which reduces the volume of the OW-PMSM system and avoids the zero sequence current [8], [9]. In addition, the HI structure can also achieve a wide speed operation range when the dc-link capacitor is well tuned to supply the reactive power. Therefore, the HI-fed OW-PMSM (HI-OW-PMSM) and its control strategy have attracted wide focus [5], [10], [11].

In recent years, finite-set model predictive control (MPC) has gained increasing attention in OW-PMSM drives due to its intuitive principle and flexibility to include multiple nonlinear constraints [12]–[15]. In the HI-OW-PMSM system, the control constraint of dc-link capacitor voltage can be included into the cost function in addition to the control of torque and flux [15]. However, since more control targets are included in MPC, the tuning work of weighting factors becomes complicated. Meanwhile, conventional MPC (C-MPC) applies only one optimal voltage vector in each control period and the steady state performance of the control system needs to be improved. In HI-OW-PMSM system, the capacitor voltage is coupled to the switching states of both inverters, so all different switching states need to be evaluated with the cost function and the calculation burden of C-MPC becomes relatively high [15].

In order to remove the complex tuning work of weighting factors in C-MPC, several low-complexity MPC strategies have been proposed. The constraints of torque and flux in the cost function are either converted into the constraint of an equivalent flux vector [16], [17], or converted into the constraint of an equivalent torque vector [18], [19], therefore, the weighting factors can be eliminated. Apart from that, [20] proposes a model predictive current control for semicontrolled OW-PMSM without weighting factor by employing the *d–q–0* components of stator current as three control constraints. It can be seen that these mentioned control constraints in the cost function are all selected from the normal state variables in the driven system, such as flux, torque or current, thus the weighting factors can be eliminated by unifying the control constraints into a single state

variable. However, in the HI-OW-PMSM system, the dc-link capacitor voltage constraint is the state of dc-link capacitor but not the state of PMSM. Because the dc-link capacitor voltage is determined and coupled to the stator current and the switching states of inverters, it is difficult to directly convert the dc-link capacitor voltage to torque, flux or current in the same way as that in the literature mentioned before.

In the OW-PMSM system, the increased number of candidate voltage vectors and switching states leads to high calculation burden of MPC and simplified MPC strategies have been investigated in [21] and [22] to reduce the number of candidate voltage vectors. In [21], the principle of DTC is combined with MPC and the number of candidate voltage vectors is reduced from 19 to 6. The optimal voltage vector is selected under A-B-C reference frame in [22] and it requires three times of evaluation in each phase and the evaluation times is reduced from 27 times to 9 times. However, in the HI-OW-PMSM system, the dc-link capacitor voltage constraint is coupled to the stator current and the switching states of the inverters [15]. The evaluation times of switching states cannot be reduced with the decreased number of the candidate voltage vectors. In order to avoid the complicated selection of candidate switching states, the dc-link capacitor voltage constraint needs to be converted as a voltage control target and be unified with other control targets in the HI-OW-PMSM system.

Apart from that, there are some modified strategies proposed to reduce the torque and flux ripples caused by single vector based MPC. A three-vector-based MPC has been proposed in [23] and the duration calculation is considered complex due to the trigonometric calculation. The trigonometric calculation is avoided in [24] and [25], but the selection of optimal voltage vectors still requires sector determination to locate the reference voltage vector. Zhang *et al.* [26] proposed a simplified multivector-based MPC method, in which the applied voltage vectors and duty ratio optimization are determined and calculated through cost function. However, the duration calculation will become complicated when there are more than two constraints in the cost function. Among the above methods, the selection and duration calculation of the optimal voltage vectors rely on the reference voltage vector. However, in the HI-OW-PMSM system, the capacitor voltage constraint cannot be converted to motor state variables and it is difficult to unify the control targets as a reference voltage vector. Moreover, the switching states of the optimal voltage vector have direct influence on the capacitor voltage and those methods mentioned above cannot be directly applied in the HI-OW-PMSM system.

The main contribution of this article is to propose an improved three-vector-based MPC (ITMPC) for the HI-OW-PMSM system by converting the capacitor voltage constraint into an energy storage form and further eliminating the weighting factors in the cost function. Based on the restructured cost function, a novel three-vector-based MPC strategy is achieved without sector division and complex calculations, which simplifies the computational burden compared with space vector modulation (SVM) MPC proposed in [26] and [27].

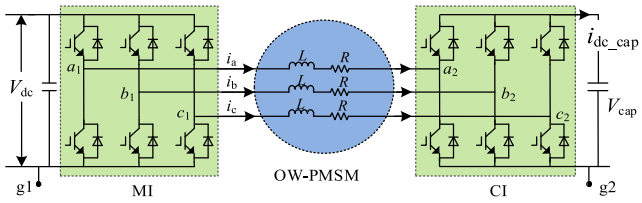

Fig. 1. Block diagram of the HI-OW-PMSM system.

II. Mathematical Model of the HI-OW-PMSM

A. Modeling of the HI System

The HI-OW-PMSM with a dc-link capacitor studied in this article is illustrated in Fig. 1, where the neutral point of the stator winding of PMSM is opened and the system is connected with a inverter fed by a dc-link voltage source $V_{\rm dc}$, named as main inverter (MI), and an inverter fed by dc-link capacitor $V_{\rm cap}$, named as conditioning inverter (CI), respectively. Due to the dc-link capacitor can supply reactive power, it can achieve a wide speed operation range by well tuning of the dc-link capacitor voltage.

Based on the Kirchhoff's laws, the voltage vector generated by the HI system in the α–β stationary reference frame can be expressed as

$$\begin{bmatrix} u_\alpha \\ u_\beta \end{bmatrix} = \frac{1}{3}\begin{bmatrix} 2 & -1 & -1 \\ 0 & 0\sqrt{3} & -\sqrt{3} \end{bmatrix}\begin{bmatrix} S_{\rm a1} \\ S_{\rm b1} \\ S_{\rm c1} \end{bmatrix} V_{\rm dc} - \frac{1}{3}\begin{bmatrix} 2 & -1 & -1 \\ 0 & \sqrt{3} & -\sqrt{3} \end{bmatrix}\begin{bmatrix} S_{\rm a2} \\ S_{\rm b2} \\ S_{\rm c2} \end{bmatrix} V_{\rm cap} \tag{1}$$

where $S_{\rm a}$, $S_{\rm b}$, and $S_{\rm c}$ denote the switching states of the three-phase leg a, b, and c, respectively (S = "1" denotes the upper leg of switch device is turn ON and the lower leg is turn OFF; S = "0" denotes the opposite).

Hence, according to (1), the voltage vector generated by the HI system is determined by outputs of both MI and CI, which can be further simplified as

$$\boldsymbol{u}_{\alpha\beta} = \boldsymbol{u}_{{\rm MI}-\alpha\beta} - \boldsymbol{u}_{{\rm CI}-\alpha\beta}. \tag{2}$$

When both inverters are two-level three-phase in this article, there are $2^3 = 8$ switching states in total corresponding to all potential 8 voltage vectors as shown in Fig. 1(a) and (b). In order to simplify the theoretical analysis, the ratio of 1:1 is employed for $V_{\rm dc}$ and $V_{\rm cap}$, and thus a three-level voltage can be produced as shown in Fig. 2(c), there are $2^3 \times 2^3 = 64$ switching states in total in the HI system.

B. Modeling of the OW-PMSM

The dynamic equations of the stator voltage, flux and torque of the OW-PMSM system in *d-q* reference frame are expressed as

$$\begin{bmatrix} u_{\rm d} \\ u_{\rm q} \end{bmatrix} = R_{\rm s}\begin{bmatrix} i_{\rm d} \\ i_{\rm q} \end{bmatrix} + p\begin{bmatrix} \Psi_{\rm d} \\ \Psi_{\rm q} \end{bmatrix} + \boldsymbol{\omega}_{\rm r}\begin{bmatrix} -\Psi_{\rm q} \\ \Psi_{\rm d} \end{bmatrix} \tag{3}$$

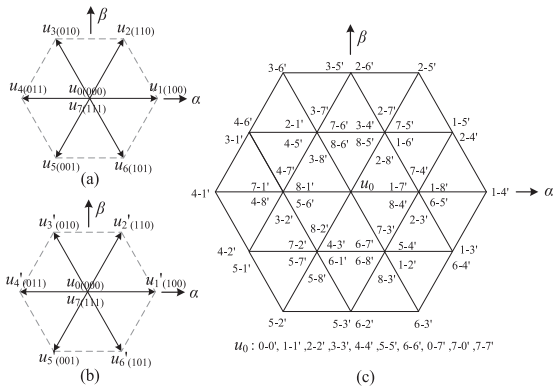

Fig. 2. Voltage vector plane of the HI system. (a) Main inverter. (b) Conditioning inverter. (c) Hybrid-inverter.

$$\begin{bmatrix}\Psi_{\rm d}\\ \Psi_{\rm q}\end{bmatrix}=\begin{bmatrix}L_{\rm d} & 0\\ 0 & L_{\rm q}\end{bmatrix}\begin{bmatrix}i_{\rm d}\\ i_{\rm q}\end{bmatrix}+\begin{bmatrix}\Psi_{\rm f}\\ 0\end{bmatrix} \tag{4}$$

$$T_{\rm e}=\frac{3}{2}N_{\rm p}\left(\Psi_{\rm d}i_{\rm q}-\Psi_{\rm q}i_{\rm d}\right) \tag{5}$$

where $u_{\rm d}$ and $u_{\rm q}$ denote the d- and q-axis component of stator voltage $\boldsymbol{u}_{\rm s}$, respectively; $R_{\rm s}$ and $\Psi_{\rm f}$ are the stator resistance and the permanent magnet flux linkage, respectively; $i_{\rm d}$ and $i_{\rm q}$ denote the d- and q-axis component of stator current $\boldsymbol{i}_{\rm s}$, respectively; p denotes the differential operator; $\Psi_{\rm d}$ and $\Psi_{\rm q}$ denote the d- and q-axis component of stator flux linkage $\boldsymbol{\Psi}_{\rm s}$, respectively; $L_{\rm d}$ and $L_{\rm q}$ denote the d- and q-axis component of the stator inductances, respectively; $\omega_{\rm r}$ is the electrical rotor speed; $T_{\rm e}$ and $N_{\rm p}$ are the electromagnetic torque and the number of pole pairs, respectively.

By discretizing the dynamic (3)–(5), the discrete model of OW-PMSM is expressed as

$$\begin{bmatrix}u_{\rm d}^{\rm k}\\ u_{\rm q}^{\rm k}\end{bmatrix}=R_{\rm s}\begin{bmatrix}i_{\rm d}^{\rm k}\\ i_{\rm q}^{\rm k}\end{bmatrix}+\frac{1}{t_{\rm s}}\begin{bmatrix}\Psi_{\rm d}^{\rm k+1}-\Psi_{\rm d}^{\rm k}\\ \Psi_{\rm q}^{\rm k+1}-\Psi_{\rm q}^{\rm k}\end{bmatrix}+\boldsymbol{\omega}_{\rm r}\begin{bmatrix}-\Psi_{\rm q}^{\rm k}\\ \Psi_{\rm d}^{\rm k}\end{bmatrix} \tag{6}$$

$$\begin{bmatrix}\Psi_{\rm d}^{\rm k+1}\\ \Psi_{\rm q}^{\rm k+1}\end{bmatrix}=\begin{bmatrix}L_{\rm d} & 0\\ 0 & L_{\rm q}\end{bmatrix}\begin{bmatrix}i_{\rm d}^{\rm k+1}\\ i_{\rm q}^{\rm k+1}\end{bmatrix}+\begin{bmatrix}\Psi_{\rm f}\\ 0\end{bmatrix} \tag{7}$$

$$T_{\rm e}^{\rm k+1}=\frac{3}{2}N_{\rm p}\left(\Psi_{\rm d}^{\rm k+1}i_{\rm q}^{\rm k+1}-\Psi_{\rm q}^{\rm k+1}i_{\rm d}^{\rm k+1}\right). \tag{8}$$

III. C-MPC FOR THE HI-OW-PMSM

In HI-OW-PMSM system, the dc-link voltage of the capacitor becomes an additional control target apart from the control of torque and flux. Therefore, the current model of capacitance voltage is used to realize control of capacitor voltage in C-MPC and additional control targets and weighting factors are introduced in the cost function.

A. Current Model of Capacitance Voltage

In [15], a current model is used to evaluate the capacitance voltage, hence the capacitance voltage constraint in cost function can be expressed related to the stator current and the current model of $V_{\rm cap}$ can be expressed as

$$\frac{dV_{\rm cap}}{dt}=i_{\rm dc\_cap}\cdot\frac{1}{C_{\rm cap}} \tag{9}$$

where $C_{\rm cap}$ denotes the dc-link floating capacitor and the $i_{\rm dc\_cap}$ can be obtained as [15]

$$i_{\rm dc\_cap}=\left\{\frac{1}{3}\begin{bmatrix}2 & -1 & -1\\ 0 & \sqrt{3} & -\sqrt{3}\end{bmatrix}\begin{bmatrix}S_{\rm a2}\\ S_{\rm b2}\\ S_{\rm c2}\end{bmatrix}\right\}^{\rm T}\begin{bmatrix}i_\alpha\\ i_\beta\end{bmatrix} \tag{10}$$

where i_α and i_β denote the α and β component of the stator current.

By discretizing (9), the discrete current model of $V_{\rm cap}$ in [15] is given by

$$V_{\rm cap}^{\rm k+1}=t_{\rm s}\cdot\frac{i_{\rm dc\_cap}^{\rm k}}{C_{\rm cap}}+V_{\rm cap}^{\rm k} \tag{11}$$

where $t_{\rm s}$ denotes the control period; the superscript "k" and "k+1" denote the system states in (k)th and (k+1) th control instant, respectively; the $i_{\rm dc\_cap}^{\rm k}$ is expressed as

$$i_{\rm dc\_cap}^{\rm k}=\left\{\frac{1}{3}\begin{bmatrix}2 & -1 & -1\\ 0 & \sqrt{3} & -\sqrt{3}\end{bmatrix}\begin{bmatrix}{S_{\rm a2}}^{\rm k}\\ {S_{\rm b2}}^{\rm k}\\ {S_{\rm c2}}^{\rm k}\end{bmatrix}\right\}^{\rm T}\begin{bmatrix}{i_\alpha}^{\rm k}\\ {i_\beta}^{\rm k}\end{bmatrix}. \tag{12}$$

B. C-MPC Based on Current Model

The basic principle of C-MPC is to select an optimal voltage vector that minimizes the cost function and thus a satisfactory system control performance can be obtained. In the HI-OW-PMSM system, the cost function of C-MPC is expressed as (13) in order to select the optimal voltage vector that has minimum tracking error of torque, stator flux and $V_{\rm cap}$

$$\begin{aligned}g_{\rm i}=&\left|\left|\boldsymbol{\Psi}_{\rm s}\right|^{\rm ref}-\left(\left|\boldsymbol{\Psi}_{\rm s}\right|^{\rm k+1}\right)_{\rm i}\right|\\&+\left|T_{\rm e}^{\rm ref}-\left(T_{\rm e}^{\rm k+1}\right)_{\rm i}\right|\boldsymbol{\lambda}_1+\left|V_{\rm cap}^{\rm ref}-\left(V_{\rm cap}^{\rm k+1}\right)_{\rm i}\right|\boldsymbol{\lambda}_2\end{aligned} \tag{13}$$

where λ_1 and λ_2 denote the weighting factors of control constraints torque $T_{\rm e}$ and dc capacitor voltage $V_{\rm cap}$, respectively; the superscript "ref" denotes the reference value; the subscript "i" denotes the future value which is corresponding to a certain voltage vector $u_{\rm i}$ when evaluating all potential vector.

By using the discrete model of (6)–(8) and (11), the system prediction model of $|\boldsymbol{\Psi}_{\rm s}|^{k+1}$, $T_{\rm e}^{\rm k+1}$ and $V_{\rm cap}^{\rm k+1}$ are derived as

$$\begin{bmatrix}\Psi_{\rm d}^{\rm k+1}\\ \Psi_{\rm q}^{\rm k+1}\end{bmatrix}=\left(I-D\boldsymbol{T}_{\rm s}\right)\begin{bmatrix}\Psi_{\rm d}^{\rm k}\\ \Psi_{\rm q}^{\rm k}\end{bmatrix}+\boldsymbol{T}_{\rm s}\begin{bmatrix}\boldsymbol{u}_{\rm d}^{\rm k}\\ \boldsymbol{u}_{\rm q}^{\rm k}\end{bmatrix}+\frac{\boldsymbol{R}_{\rm s}\boldsymbol{t}_{\rm s}}{\boldsymbol{L}_{\rm d}}\begin{bmatrix}\Psi_{\rm f}\\ 0\end{bmatrix} \tag{14}$$

$$\begin{bmatrix}{\boldsymbol{i}_{\rm d}}^{\rm k+1}\\ {\boldsymbol{i}_{\rm q}}^{\rm k+1}\end{bmatrix}=\mathbf{E}\left(\begin{bmatrix}\Psi_{\rm d}^{\rm k+1}\\ \Psi_{\rm q}^{\rm k+1}\end{bmatrix}-\begin{bmatrix}\Psi_{\rm f}\\ 0\end{bmatrix}\right) \tag{15}$$

$$\begin{cases}\left|\boldsymbol{\Psi}_{\rm s}\right|^{\rm k+1}=\sqrt{\left(\Psi_{\rm d}^{\rm k+1}\right)^2+\left(\Psi_{\rm q}^{\rm k+1}\right)^2}\\ T_{\rm e}^{\rm k+1}=\frac{3}{2}N_{\rm p}\left(\Psi_{\rm d}^{\rm k+1}i_{\rm q}^{\rm k+1}-\Psi_{\rm q}^{\rm k+1}i_{\rm d}^{\rm k+1}\right)\end{cases} \tag{16}$$

$$V_{\rm cap}^{\rm k+1}=t_{\rm s}\cdot i_{\rm dc\_cap}^{\rm k}/C_{\rm cap}+V_{\rm cap}^{\rm k} \tag{17}$$

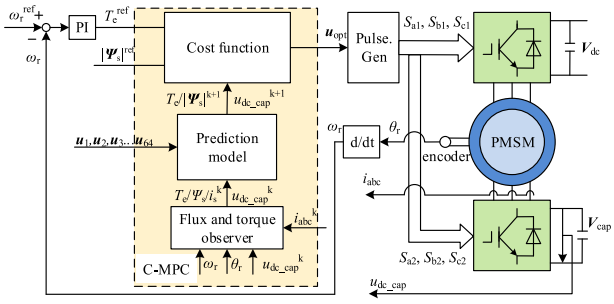

Fig. 3. Control block diagram of the C-MPC for the HI-OW-PMSM system.

where $\mathrm{D}=\left[\begin{smallmatrix}R_s/L_d & -\omega_r \\ \omega_r & R_s/L_q\end{smallmatrix}\right]$; $\mathrm{E}=\left[\begin{smallmatrix}1/L_d & 0 \\ 0 & 1/L_q\end{smallmatrix}\right]$; $\boldsymbol{I}$ is the identity matrix.

According to the voltage vector plane of the HI system in Fig. 2(c), there exists 64 different switching states and 64 potential voltage vectors. Hence, by using the prediction model (14)–(17), it will generate 64 possible prediction results $(|\boldsymbol{\Psi}_s|^{k+1})_i$, $(T_e^{k+1})_i$ and $(V_{cap}^{k+1})_i$, where i = 12 …64.

Finally, by substituting all 64 prediction results into the cost function (13), the switching state that minimizes the cost function is selected as the optimal one, and thus the corresponding voltage vector is selected. The control block diagram of C-MPC for HI-OW-PMSM is shown in Fig. 3.

It can be seen that the procedure of voltage selection is time consuming and with high calculation burden because of the prediction and evaluation work of all 64 voltage vectors. Furthermore, a considerable static ripple will be obtained in the C-MPC because employing a single voltage vector during each control period. Besides, the existence of the capacitance voltage constraint will further expand the divergence between the selected voltage vector and the reference voltage vector, hence deteriorates the dynamic and steady state performance of C-MPC. Meantime, in order to ensure stable control of capacitor voltage, the complex weighting factors tuning work for two weighting factors is needed for C-MPC.

On the other hand, multivector-based MPC method is difficult to employ in HI-OW-PMSM to suppress the torque ripple. Since V_{cap} is coupled to the stator current and the switching states of inverters, as shown in (10) and (11), it is difficult to calculate the voltage reference by dead-beat method or determine the optimal voltage vector as that in [23], [24], and [28]. Therefore, simplified voltage selection and duration calculation schemes are difficult to achieve. Moreover, the dc-link capacitor voltage constraint is difficult to be directly converted into torque, flux or current for the purpose of eliminating these two weighting factors. Thus, it is necessary to reconstruct the predictive model and the cost function to realize simple multi-vector based MPC control.

IV. Proposed ITMPC Method

In this section, a new prediction model of V_{cap} is proposed and the two weighting factors in the cost function can be eliminated. Accordingly, by using the new prediction model, a voltage reference is obtained and an improved three-vector prediction strategy without sector division can be carried out to achieve the three optimal voltage vectors and their duty cycles, which improves the torque control performance and reduce the system calculation burden effectively.

A. New Prediction Model Based on Energy Storage Model

In order to decouple the V_{cap} from the stator current and inverter switching states, a new prediction model based on energy is proposed. The energy stored in V_{cap} can be expressed as

$$W_{cap}=\frac{1}{2}C_{cap}\cdot V_{cap}^2 \tag{18}$$

where W_{cap} denotes the energy stored in V_{cap}. Therefore, the fluctuation of W_{cap} during one sampling period can be calculated as

$$\Delta W_{cap}=\frac{1}{2}C_{cap}\left[\left(V_{cap}^{k+1}\right)^2-\left(V_{cap}^{k}\right)^2\right]. \tag{19}$$

Meanwhile, the active power P flows through CI can be expressed as

$$P=\boldsymbol{u}_{CI\_act}\cdot|\boldsymbol{i}_s| \tag{20}$$

where u_{CI_act} denotes the active component of CI output voltage; $|\boldsymbol{i_s}|$ denotes the amplitude of stator current vector; $P\geq 0$ denotes the active power flows from C_{cap} to PMSM and $P<0$ denotes the active power flows from PMSM to C_{cap}.

Since the intrinsic of W_{cap} fluctuation is caused by the active power flowing from the CI, the ΔW_{cap} can be further expressed by substituting (20) into (19), as follows:

$$\begin{aligned}\Delta W_{cap}&=\frac{1}{2}C_{cap}\left[\left(V_{cap}^{k+1}\right)^2-\left(V_{cap}^{k}\right)^2\right]\\&=P\cdot t_s\cdot n=\boldsymbol{u}_{CI\_act}\cdot|\boldsymbol{i}_s|\cdot t_s\cdot n\end{aligned} \tag{21}$$

where $n = 1, 2, 3\ldots$ denotes the charging step.

Hence, a new prediction model of V_{cap}^{k+1} can be derived from (21) and expressed as

$$V_{cap}^{k+1}=\sqrt{\left(V_{cap}^{k}\right)^2+\left(\boldsymbol{u}_{CI\_act}{}^{k}\cdot|\boldsymbol{i}_s|^{k}\cdot 2\right)/C_{cap}}. \tag{22}$$

B. Novel Cost Function

In order to eliminated the weighting factor for torque constraint, $i_d = 0$ control mode is employed. According to [28], cost function (13) can be simplified as

$$\begin{aligned}g_i=&\left|\Psi_d^{ref}-\Psi_d^{k+1}\right|+\left|\Psi_q^{ref}-\Psi_q^{k+1}\right|\\&+\lambda\left|V_{cap}^{ref}-V_{cap}^{k+1}\right|.\end{aligned} \tag{23}$$

It can be seen from (23) the weighting factor for capacitance voltage constraint still exists. In order to further simplify the cost function to realize multivector MPC, the energy prediction model is employed to eliminate the weighting factor.

Based on the principle of MPC, the optimal voltage vector is the vector that minimizing the cost functions. It can be seen from (23) that the cost function g_i will get minimum (equals to zero) when $\Psi_{d/q}^{k+1}$ and V_{cap}^{k+1} equal to their references $\Psi_{d/q}^{ref}$ and

$V_{\mathrm{cap}}^{\mathrm{ref}}$. Hence, combining (14) and (23), the minimum condition is expressed as

$$\begin{cases} \boldsymbol{\Psi}_{\mathrm{d}}^{\mathrm{ref}}=\boldsymbol{\Psi}_{\mathrm{d}}^{\mathrm{k+1}}=\boldsymbol{\Psi}_{\mathrm{d}}^{\mathrm{k}}+u_{\mathrm{d}}^{\mathrm{k}}\cdot t_{\mathrm{s}}+\left(\omega_{\mathrm{r}}\boldsymbol{\Psi}_{\mathrm{q}}^{\mathrm{k}}-R_{\mathrm{s}}i_{\mathrm{d}}^{\mathrm{k}}\right)\cdot t_{\mathrm{s}} \\ \boldsymbol{\Psi}_{\mathrm{q}}^{\mathrm{ref}}=\boldsymbol{\Psi}_{\mathrm{q}}^{\mathrm{k+1}}=\boldsymbol{\Psi}_{\mathrm{q}}^{\mathrm{k}}+u_{\mathrm{q}}^{\mathrm{k}}\cdot t_{\mathrm{s}}-\left(\omega_{\mathrm{r}}\boldsymbol{\Psi}_{\mathrm{d}}^{\mathrm{k}}+R_{\mathrm{s}}i_{\mathrm{q}}^{\mathrm{k}}\right)\cdot t_{\mathrm{s}} \\ V_{\mathrm{cap}}^{\mathrm{ref}}=V_{\mathrm{cap}}^{\mathrm{k+1}}=\sqrt{\left(V_{\mathrm{cap}}^{\mathrm{k}}\right)^2+\left(u_{\mathrm{CI\_act}}{}^{\mathrm{k}}\cdot|\boldsymbol{i}_{\mathrm{s}}|^{\mathrm{k}}\cdot 2\right)\Big/C_{\mathrm{cap.}}} \end{cases} \tag{24}$$

By solving (24), the voltage vector $\boldsymbol{u}_{\mathrm{s}}^{\mathrm{ref}}$ and $u_{\mathrm{CI\_act}}^{\mathrm{ref}}$ that make both $\Psi_{\mathrm{d/q}}^{\mathrm{k+1}}$ and $V_{\mathrm{cap}}^{\mathrm{k+1}}$ following their references without errors are obtained as

$$\begin{cases} \boldsymbol{u}_{\mathrm{d}}^{\mathrm{ref}}=\left(\boldsymbol{\Psi}_{\mathrm{d}}^{\mathrm{ref}}-\boldsymbol{\Psi}_{\mathrm{d}}^{\mathrm{k}}\right)/t_{\mathrm{s}}+R_{\mathrm{s}}i_{\mathrm{d}}^{\mathrm{k}}-\omega_{\mathrm{r}}\boldsymbol{\Psi}_{\mathrm{q}}^{\mathrm{k}} \\ \boldsymbol{u}_{\mathrm{q}}^{\mathrm{ref}}=\left(\boldsymbol{\Psi}_{\mathrm{q}}^{\mathrm{ref}}-\boldsymbol{\Psi}_{\mathrm{q}}^{\mathrm{k}}\right)/t_{\mathrm{s}}+R_{\mathrm{s}}i_{\mathrm{q}}^{\mathrm{k}}+\omega_{\mathrm{r}}\boldsymbol{\Psi}_{\mathrm{d}}^{\mathrm{k}} \\ \boldsymbol{u}_{\mathrm{CI}\_act}^{\mathrm{ref}}=\left[\left(V_{\mathrm{cap}}^{\mathrm{ref}}\right)^2-\left(V_{\mathrm{cap}}^{\mathrm{k}}\right)^2\right]\cdot C_{\mathrm{cap}}/\left(2\cdot i_{\mathrm{s}}^{\mathrm{k}}\cdot t_{\mathrm{s}}\right) \end{cases} \tag{25}$$

where $u_{\mathrm{d}}^{\mathrm{ref}}$ and $u_{\mathrm{q}}^{\mathrm{ref}}$ denote the *d* and *q* component of system output voltage vector reference $u_{\mathrm{s}}^{\mathrm{ref}}$; $u_{\mathrm{CI\_act}}^{\mathrm{ref}}$ denotes the reference of the active component of CI output voltage. That is to say, if the HI outputs the $\boldsymbol{u}_{\mathrm{s}}^{\mathrm{ref}}$ and the reactive component of CI is equal to $u_{\mathrm{CI\_act}}^{\mathrm{ref}}$, the system will perform with no tracking error. Furthermore, it can be seen from (14) and (22) that the predictive $\Psi_{\mathrm{d}}^{\mathrm{k+1}}$, $\Psi_{\mathrm{q}}^{\mathrm{k+1}}$ and $u_{\mathrm{dc\_cap}}^{\mathrm{k+1}}$ increase monotonously with the increase of u_{d}, u_{q} and $u_{\mathrm{CI\_act}}$. Hence, the tracking errors of $\Psi_{\mathrm{d/q}}$ and V_{cap} are equivalent to the tracking errors of $u_{\mathrm{d/q}}$ and $u_{\mathrm{CI\_act}}$.

In this way, the cost function g_{i} can be further simplified as (26), where the torque and flux control constraints are replaced by the *d* and *q* component of stator voltage vector

$$\begin{aligned} c_{\mathrm{i}}=&\left|\boldsymbol{u}_{\mathrm{d}}^{\mathrm{ref}}-\boldsymbol{u}_{\mathrm{d}}^{\mathrm{k+1}}\right| \\ &+\left|\boldsymbol{u}_{\mathrm{q}}^{\mathrm{ref}}-\boldsymbol{u}_{\mathrm{q}}^{\mathrm{k+1}}\right|+\left|u_{\mathrm{CI}\_act}{}^{\mathrm{ref}}-u_{\mathrm{CI}\_act}{}^{\mathrm{k+1}}\right|. \end{aligned} \tag{26}$$

It can be seen from (26) that the weighting factors in the novel cost function have been effectively eliminated by introducing the new prediction model of the capacitor voltage. Using the novel cost function, it is feasible to further apply a three vector scheme in MPC for the HI-OW-PMSM system.

C. Voltage Reference Distribution Between Two Inverters

As discussed previously, the basic principle of C-MPC is transformed to determine the voltage vector that minimizing the tracking error of $u_{\mathrm{d,q}}$ and $u_{\mathrm{CI\_act}}$ with their references. However, the CI mainly supplies reactive voltage and requires active voltage to maintain the V_{cap}, and thus the MI supplies the whole active voltage and the rest of reactive voltage when CI could not supply all the required reactive voltage.

Hence, the reference value calculated in (25) needs to be distributed to both MI and CI to ensure the optimal output voltages of MI and CI. The voltage reference distribution is shown as Fig. 4, where subscript "act" and "rea" denote the active and reactive voltage component, respectively; θ_{i} denotes the angle of the stator current $\boldsymbol{i}_{\mathrm{s}}$; CI limiter is to prevent the voltage reference of CI from exceeding its maximum value.

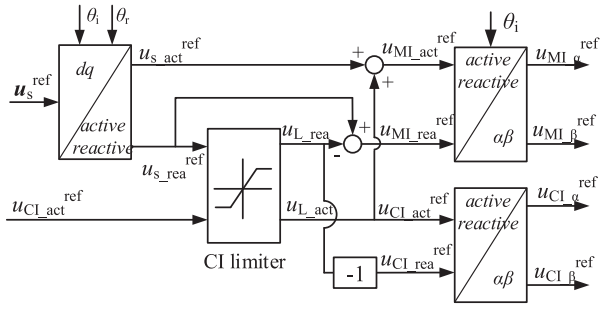

Fig. 4. Schematic diagram of voltage reference distribution of MI and CI.

According to the value of V_{cap}, the CI limiter is expressed as following two cases.

1) When $\sqrt{\left(u_{\mathrm{s\_rea}}{}^{\mathrm{ref}}\right)^2+\left(u_{\mathrm{CI\_act}}{}^{\mathrm{ref}}\right)^2}\le \mathbf{V}_{\mathrm{cap}}/\sqrt{3}$, that is to say, the CI is able to supply the whole system reactive voltage, the output of CI limiter is obtained as

$$\begin{cases} u_{\mathrm{L\_act}}=u_{\mathrm{CI\_act}}{}^{\mathrm{ref}} \\ u_{\mathrm{L\_rea}}=u_{\mathrm{s\_rea}}{}^{\mathrm{ref}}. \end{cases} \tag{27}$$

2) When $\sqrt{\left(u_{\mathrm{s\_rea}}{}^{\mathrm{ref}}\right)^2+\left(u_{\mathrm{CI\_act}}{}^{\mathrm{ref}}\right)^2}>\mathbf{V}_{\mathrm{cap}}/\sqrt{3}$, that is to say, the CI is unable to supply the whole system reactive voltage, the output of CI limiter is obtained as

$$\begin{cases} u_{\mathrm{L\_act}}=\boldsymbol{u}_{\mathrm{CI\_act}}{}^{\mathrm{ref}} \\ u_{\mathrm{L\_rea}}=\sqrt{\left(V_{\mathrm{cap}}/\sqrt{3}\right)^2-\left(u_{\mathrm{CI\_act}}{}^{\mathrm{ref}}\right)^2}. \end{cases} \tag{28}$$

The transformation of *dq* to active/reactive is expressed as

$$\begin{bmatrix} u_{\mathrm{act}} \\ u_{\mathrm{rea}} \end{bmatrix}=\begin{bmatrix} \cos\left(\theta_{\mathrm{i}}-\theta_{\mathrm{r}}\right) & \sin\left(\theta_{\mathrm{i}}-\theta_{\mathrm{r}}\right) \\ -\sin\left(\theta_{\mathrm{i}}-\theta_{\mathrm{r}}\right) & \cos\left(\theta_{\mathrm{i}}-\theta_{\mathrm{r}}\right) \end{bmatrix}\begin{bmatrix} u_{\mathrm{d}} \\ u_{\mathrm{q}} \end{bmatrix}. \tag{29}$$

The transformation of active/reactive to $\alpha\beta$ is expressed as

$$\begin{bmatrix} u_{\alpha} \\ u_{\beta} \end{bmatrix}=\begin{bmatrix} \sin\left(\theta_{\mathrm{i}}\right) & -\cos\left(\theta_{\mathrm{i}}\right) \\ \cos\left(\theta_{\mathrm{i}}\right) & \sin\left(\theta_{\mathrm{i}}\right) \end{bmatrix}\begin{bmatrix} u_{\mathrm{act}} \\ u_{\mathrm{rea}} \end{bmatrix}. \tag{30}$$

Hence, the reference $u_{\mathrm{s}}^{\mathrm{ref}}$ and $u_{\mathrm{CI\_act}}^{\mathrm{ref}}$ are divided into $\boldsymbol{u}_{\mathrm{MI}}^{\mathrm{ref}}$ and $\boldsymbol{u}_{\mathrm{CI}}^{\mathrm{ref}}$ efficiently.

D. Three-Vector Strategy Without Sector Division

After obtaining the reference $u_{\mathrm{MI}}^{\mathrm{ref}}$ and $u_{\mathrm{CI}}^{\mathrm{ref}}$, each inverter (MI and CI) is required to determine an optimal voltage that has the lowest tracking error with the reference to achieve the good dynamic and steady-state performance. In order to improve the control performance, three-vector can be adopted. The multivector-based MPC usually require complex calculations or SVM calculation procedures, which will introduce additional sector division work. In order to reduce the large calculation burden of the conventional SVM-based multivector scheme [26], [27], an improved three-vector strategy without sector division is proposed in this article.

It can be seen from Fig. 2 that both MI and CI have the same hexagon voltage plane. Therefore, for a certain reference $\boldsymbol{u}_{\mathrm{MI}}^{\mathrm{ref}}$ or $\boldsymbol{u}_{\mathrm{CI}}^{\mathrm{ref}}$, the determination work of three vectors in both MI and CI

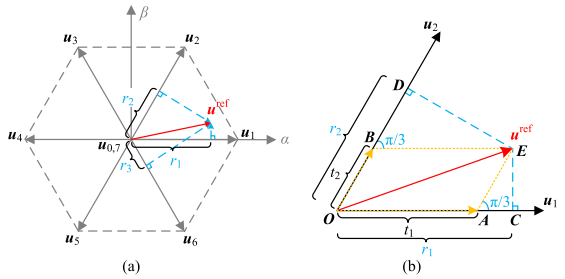

Fig. 5. Basic principle of the proposed three-vector simplified strategy.

TABLE I
VECTOR PROJECTION OF $\boldsymbol{U}^{\mathrm{ref}}$ TO SIX VECTOR

Basic vector	Vector projection	The order of the projection
$\boldsymbol{u}_1$	r_1	1
$\boldsymbol{u}_2$	r_2	2
$\boldsymbol{u}_3$	r_3	3
$\boldsymbol{u}_4$	$-r_1$	6
$\boldsymbol{u}_5$	$-r_2$	5
$\boldsymbol{u}_6$	$-r_3$	4

are the same. Taking a normal hexagon voltage plane as example, Fig. 5(a) shows the basic principle of the proposed three-vector strategy, where the red line denotes the voltage reference $\boldsymbol{u}^{\mathrm{ref}}$ (such as $\boldsymbol{u}_{\mathrm{MI}}^{\mathrm{ref}}$ or $\boldsymbol{u}_{\mathrm{CI}}^{\mathrm{ref}}$). The blue lines r_1, r_2, and r_3 denote the vector projection of $\boldsymbol{u}^{\mathrm{ref}}$ to $\boldsymbol{u}_1$, $\boldsymbol{u}_2$, and $\boldsymbol{u}_3$, respectively, which is calculated as

$$\begin{cases} r_{\boldsymbol{1}} = \dfrac{\boldsymbol{u}^{\mathbf{ref}}\cdot\boldsymbol{u_1}}{|\boldsymbol{u_1}|} = \dfrac{u_\alpha{}^{\mathbf{ref}}\cdot u_{\mathbf{1}\alpha}+u_\beta{}^{\mathbf{ref}}\cdot u_{\mathbf{1}\beta}}{2/3\cdot V_{\mathrm{dc}}} \\ r_{\boldsymbol{2}} = \dfrac{\boldsymbol{u}^{\mathbf{ref}}\cdot\boldsymbol{u_2}}{|\boldsymbol{u_2}|} = \dfrac{u_\alpha{}^{\mathbf{ref}}\cdot u_{\mathbf{2}\alpha}+u_\beta{}^{\mathbf{ref}}\cdot u_{\mathbf{2}\beta}}{2/3\cdot V_{\mathrm{dc}}} \\ r_{\boldsymbol{3}} = \dfrac{\boldsymbol{u}^{\mathbf{ref}}\cdot\boldsymbol{u_2}}{|\boldsymbol{u_3}|} = \dfrac{u_\alpha{}^{\mathbf{ref}}\cdot u_{\mathbf{3}\alpha}+u_\beta{}^{\mathbf{ref}}\cdot u_{\mathbf{3}\beta}}{2/3\cdot V_{\mathrm{dc}}} \end{cases} \tag{31}$$

where V_{dc} denotes the dc-link voltage.

Therefore, it is easy to conclude that the vector projection of $\boldsymbol{u}^{\mathrm{ref}}$ to $\boldsymbol{u}_4$, $\boldsymbol{u}_5$ and $\boldsymbol{u}_6$ is $-r_1$, $-r_2$ and $-r_3$, respectively. Table I gives all vector projections of $\boldsymbol{u}^{\mathrm{ref}}$ to six basic vector and the order of the projections amplitudes.

Then, the proposed strategy is implemented as follow:

First, the three vector chosen in the next control period should be determined. According to Fig. 5(b), the applied vectors should be selected as $\boldsymbol{u}_1$, $\boldsymbol{u}_2$, and $\boldsymbol{u}_0$. It can be seen from Table I that the applied vectors $\boldsymbol{u}_1$ and $\boldsymbol{u}_2$ correspond to the two vectors with the highest projections amplitudes. Accordingly, it can be concluded that the three optimal voltage vectors consist of two voltage vector with the largest vector projection value and a zero voltage vector.

Second, determine the duty cycles of three vectors. In order to synthesize $\boldsymbol{u}^{\mathrm{ref}}$ without error, the duty cycles of $\boldsymbol{u}_0$, $\boldsymbol{u}_1$, and $\boldsymbol{u}_2$ are $t_{\mathrm{s}}-t_1-t_2$, t_1, and t_2 according to Fig. 5(b). Due to $\angle\mathrm{DOC} = \angle\mathrm{EAC} = \angle\mathrm{EBD} = \pi/3$, the relationship of t_1, t_2 and r_1, r_2 are expressed as

$$\begin{cases} r_1 = \left(t_1 + \frac{t_2}{2}\right)\cdot|\boldsymbol{u}_1| \\ r_2 = \left(t_2 + \frac{t_1}{2}\right)\cdot|\boldsymbol{u}_2|. \end{cases} \tag{32}$$

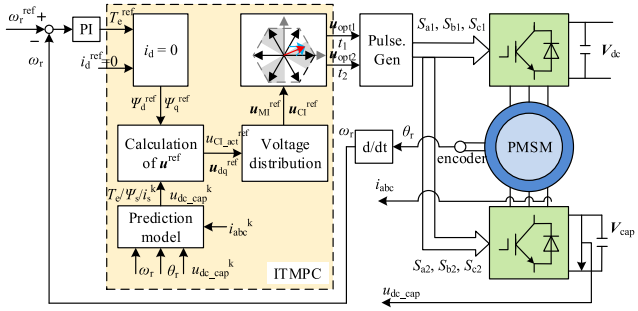

Fig. 6. Control block diagram of the ITMPC for the HI-OW-PMSM system.

Solving (33), the duty cycles of $\boldsymbol{u}_1$ and $\boldsymbol{u}_2$ are expressed as

$$\begin{cases} t_1 = (2r_1 - r_2)\cdot\frac{2}{3}/|\boldsymbol{u}_1| = (2r_1 - r_2)/V_{\mathrm{dc}} \\ t_2 = (2r_2 - r_1)\cdot\frac{2}{3}/|\boldsymbol{u}_2| = (2r_2 - r_1)/V_{\mathrm{dc}} \end{cases} \tag{33}$$

where t_1 and t_2 correspond to $\boldsymbol{u}_1$ and $\boldsymbol{u}_2$, respectively. Hence, in other random conditions, the duty cycles of two optimal vectors can be directly calculated by (33).

Finally, the working time of $\boldsymbol{u}_0$, $\boldsymbol{u}_1$, and $\boldsymbol{u}_2$ are $(t_{1*}t_{\mathrm{s}})$, $(t_{2*}t_{\mathrm{s}})$, and $(t_{\mathrm{s}}-t_1-t_2)_*t_{\mathrm{s}}$, respectively. Due to the fact that the r_1, r_2, and r_3 can be directly calculated after obtaining $\boldsymbol{u}^{\mathrm{ref}}$, the optimal voltage vectors and their duty cycles can be immediately obtained by using (31) and (33), which can be achieved without sector division work.

The whole procedure can be summarized as follows.

1) Calculate the r_1, r_2, r_3 by using (31) and then obtain the vector projection of $\boldsymbol{u}^{\mathrm{ref}}$ to all basic voltage vectors.
2) Select two voltage vectors $\boldsymbol{u}_{\mathrm{x}}$, $\boldsymbol{u}_{\mathrm{y}}$ with the largest value of vector projection r_{x}, r_{y} and $\boldsymbol{u}_0$ as the three optimal vectors.
3) Determine duty cycles of two optimal vectors $\boldsymbol{u}_{\mathrm{x}}$, $\boldsymbol{u}_{\mathrm{y}}$ by using (33): $(2r_{\mathrm{x}} - r_{\mathrm{y}})/V_{\mathrm{dc}}$ and $(2r_{\mathrm{y}} - r_{\mathrm{x}})/ < V_{\mathrm{dc}}$.
4) The duty cycle of $\boldsymbol{u}_0$ is $t_{\mathrm{s}} - t_{\mathrm{x}} - t_{\mathrm{y}}$.

E. Control Block Diagram of Proposed Method

The control block diagram of proposed method is illustrated in Fig. 6, which includes the new prediction model and the three-vector prediction strategy.

It can be seen that the weighting factor is eliminated in the new cost function. Moreover, according to the new cost function, the three optimal voltage vectors and their duty cycle are easily determined by only twice simple calculation (31) and (33). Thus, the system control complexity is extremely reduced.

V. EXPERIMENTAL RESULTS

To verify the validity and effectiveness of the proposed ITMPC, comparative experimental studies are carried out on the ITMPC, the SVM-MPC using the new mathematical model and the novel cost function proposed in this article and the modulation method proposed in [27] and the C-MPC methods for the HI-OW-PMSM. The parameters of the PMSM system are given in Table II. The experimental platform is shown in Fig. 7 and the experimental results are shown in Figs. 8 –14.

TABLE II
PARAMETERS OF OW-PMSM SYSTEM

System Parameters	Value
Stator d-axis inductance, L_d	5.86mH
Stator q-axis inductance, L_q	11.05mH
PM flux linkage, ψ_f	0.1543wb
Stator resistance, R_s	1.35Ω
Dc bus voltage, V_{dc}	90V
Poles, N_p	4
Rated power, P_n	1.3KW
Rated speed, N	2500rpm
Rated current, I_a	7.07A
Moment of inertia, J	0.00109kg·m^2.

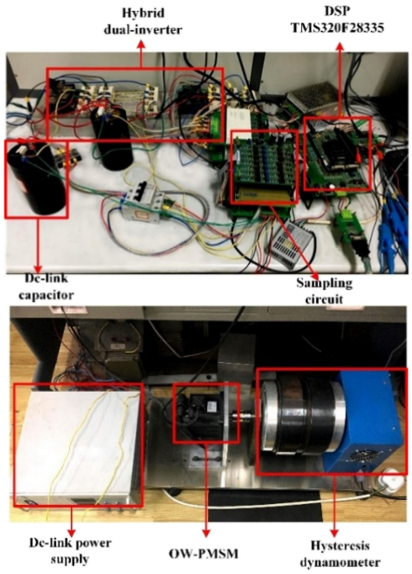

Fig. 7. Experimental platform of the HI-OW-PMSM system.

A. Experimental Steady-State Performance

The steady-state performance of rotor speed N, stator current I_a, torque T_e, and $V_{\rm cap}$ of three methods are shown in Fig. 8(a)–(c), respectively, when the system control period is 200 μs. It can be seen that the torque ripple for the ITMPC and SVM-MPC are both smaller and the currents are both more sinusoidal than C-MPC. And the steady-state performance for ITMPC is better than SVM-MPC.

In addition, it can also be seen that the proposed ITMPC method has a better steady-state control performance when the system control period is 100 μs as shown in Fig. 8(c). However, limited by high algorithm complexity of C-MPC, the C-MPC cannot work when the system control period is 100 μs in this platform. Hence, it can be concluded that the ITMPC is more practical than the C-MPC.

The FFT analyses of current and torque ripple for three strategies under 200 μs control period are given in Fig. 9. It can be seen that the total harmonic distortion (THD) of stator current has reached 35.54% and the THD of torque ripple has reached

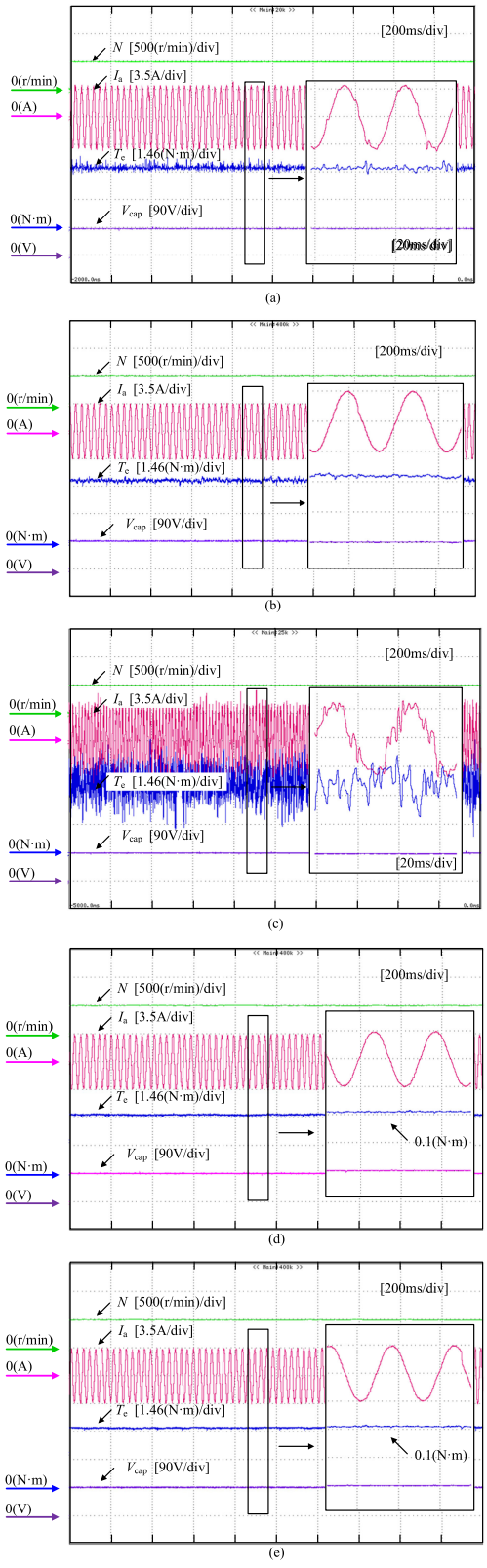

Fig. 8. Control static performance at 500 r/min with the load of 3N·m. (a) ITMPC (200 μs). (b) SVM-MPC (200 μs) (c) C-MPC (200 μs). (d) ITMPC (100 μs). (e) SVM-MPC (100 μs).

25.30% in C-MPC, which is because that only a single voltage vector is applied. The THD of stator current is 9.94% and the THD of torque ripple is 7.27% in SVM-MPC. In addition, the

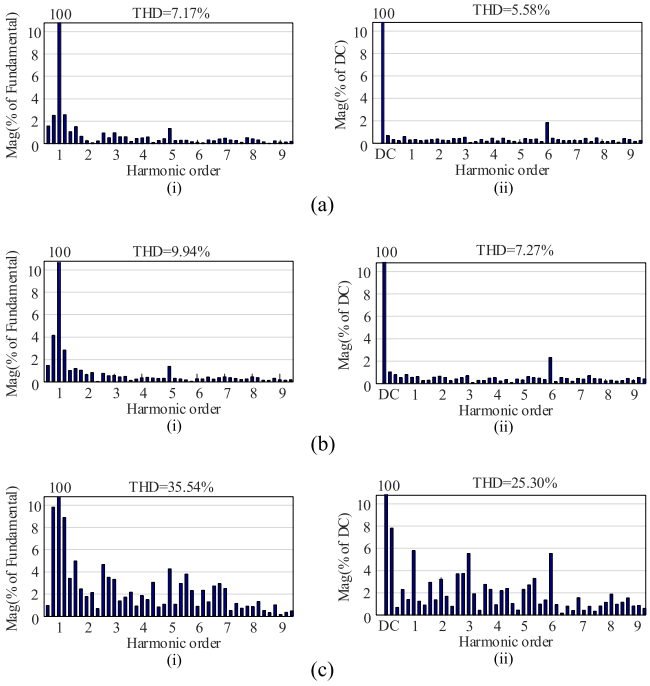

Fig. 9. FFT analysis for the stator current and torque ripple (a-i) i_a analysis for ITMPC (200 μs), (a-ii) torque ripple analysis for ITMPC (200 μs). (b-i) i_a analysis for SVM-MPC (200 μs), (b-ii) torque ripple analysis for SVM-MPC (200 μs). (c-i) i_a analysis for C-MPC (200 μs), (c-ii) torque ripple analysis for C-MPC (200 μs).

THD of stator current and torque ripple are further reduced in ITMPC.

B. Experimental Dynamic Performance

The experimental dynamic response of torque and rotor speed for three methods are shown in Fig. 10 with torque load changes from 0 to 3 N·m and Fig. 11 with the rotor speed reference steps from 250 to 750 r/min, respectively. It can be seen from Fig. 10 that the dynamic process are 3.6 and 3.9 s for ITMPC and SVM-MPC, respectively. Both are faster than that of the C-MPC with dynamic process of 4.5 s. It can be seen from Fig. 11 that the dynamic process are 1.7 s in ITMPC and 1.8 s in SVM-MPC. Both are still faster than C-MPC where the dynamic process is 2.6 s. Besides, there is less overshoot for speed and torque response in ITMPC and SVM-MPC than C-MPC.

It can also be seen that the capacitor voltages are all controlled stable in dynamic process for three methods. Which means that good dynamic performance and capacitor voltage stability can be guaranteed at the same time for SVM-MPC and ITMPC.

C. Experimental Performance When $V_{\rm cap}$ Reference Changes

In addition, in the HI-OW-PMSM system, the $V_{\rm cap}$ reference requires to be changed when it requires a lot reactive power to compensate power supply voltage drop.

Fig. 12(a) and (b) shows the dynamic performance when $V_{\rm cap}$ reference steps from 90 to 50 V (50 to 90 V) of both methods. It can be seen that the charging of $V_{\rm cap}$ will lead to a torque fluctuation because that a lot of active power flows into $C_{\rm cap}$. In this condition, by tuning the charging step n in (21), the ITMPC can charge the $V_{\rm cap}$ in a gentle way, which is shown in Fig. 12(c). Therefore, it can be concluded that the ITMPC is more flexible than C-MPC.

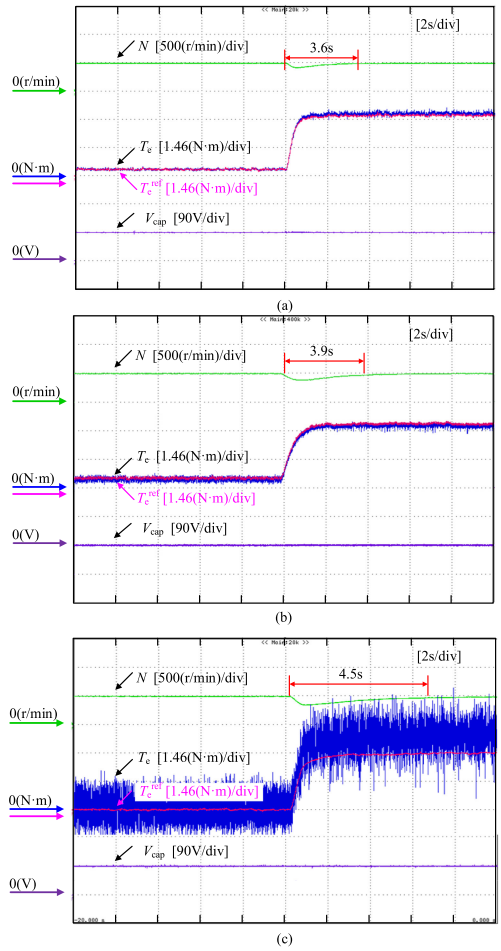

Fig. 10. Dynamic performance when the load changes from 0 to 3 N·m of three methods. (a) Improved three-vector-based model predictive control. (b) Space vector modulation - model predictive control. (c) Conventional model predictive control.

D. Comparative Analysis for Three Methods

Fig. 13 shows the calculation time of ITMPC, SVM-MPC, and C-MPC method during each control period. It can be seen that the calculation time of ITMPC is lower than SVM-MPC and C-MPC, which indicates that the ITMPC significantly simplifies the iterative calculation of C-MPC and SVM calculation procedure of SVM-MPC and reduce the system calculation burden.

The comparison of C-MPC, SVM-MPC, and ITMPC is given in Table III. Since both SVM-MPC and ITMPC are based on the new mathematical model and the novel cost function proposed in this article, so the ITMPC and SVM-MPC have similar steady state and dynamic performance. The current harmonic and torque ripple for the ITMPC are slightly improved compared with SVM-MPC due to that the ITMPC avoids the sector division and simplifies the modulation calculation procedures. Thus, the calculation time of ITMPC is also shorter than SVM-MPC.

TABLE III
COMPARISON OF ITMPC, C-MPC, AND SVM-MPC

	C-MPC	SVM-MPC	ITMPC
THD of stator current	35.54%	9.94%	7.17%
THD of torque ripples	25.30%	7.27%	5.58%
Dynamic Performance with load changes	4.5s	3.9s	3.6s
Dynamic Performance with speed changes	2.6s	1.8s	1.7s
Calculation time	165μs	50μs	41μs
Switching frequency	1.8kHz	9.6kHz	9.7kHz

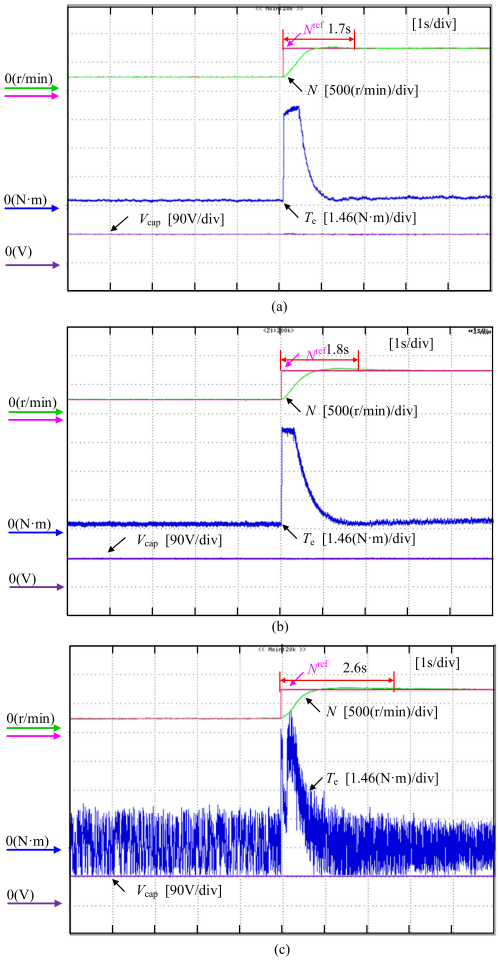

Fig. 11. Dynamic performance when the rotor speed reference steps from 250 to 500 r/min of three methods. (a) Improved three-vector-based MPC. (b) Space vector modulation model predictive control. (c) Conventional model predictive control.

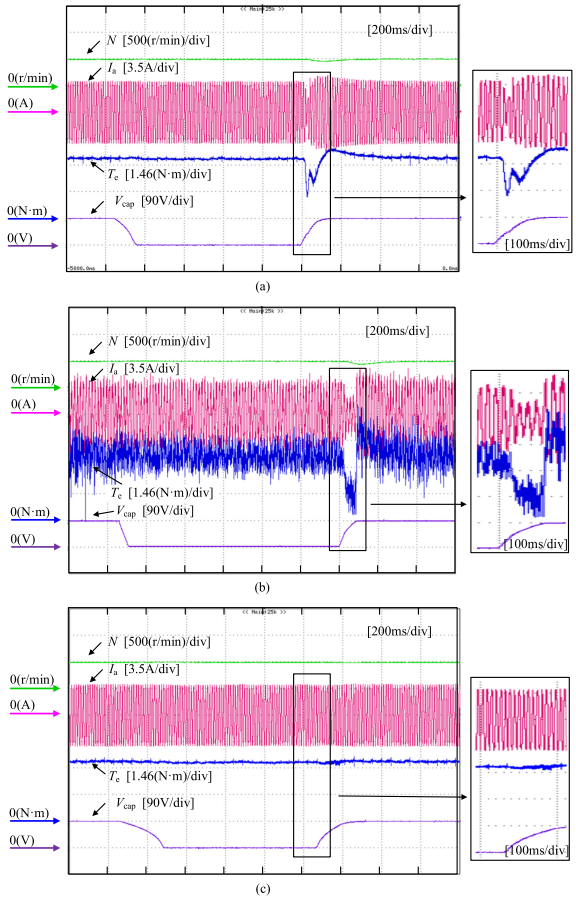

Fig. 12. Dynamic performance when $V_{\rm cap}$ reference steps from 90 V(50 V) to 50 V(90 V). (a) ITMPC ($n = 1$). (b) Conventional model predictive control. (c) ITMPC($n = 3$).

Meanwhile, the average switching frequency for three methods with the same sampling period is provided. It can be seen that the switching frequency of SVM-MPC and ITMPC are both higher than C-MPC due to that multivectors are applied in each control period.

In order to validate that the proposed SVM-MPC and ITMPC has better control performance than C-MPC under the same switching frequency. The sampling frequencies of SVM-MPC and ITMPC are reset as 0.94 and 0.92 kHz. Thus, the switching frequencies for SVM-MPC and ITMPC are both 1.8 kHz, which is the same as that of C-MPC shown in Fig. 8(c). The experimental results are presented in Fig. 14.

It can be seen that due to the reduction of sampling frequency, the performances of both SVM-MPC and ITMPC are all deteriorated. However, they are still better than that of C-MPC as shown in Fig. 8(c). Thus, it can be concluded that the proposed ITMPC and SVM-MPC have better performance than the C-MPC in

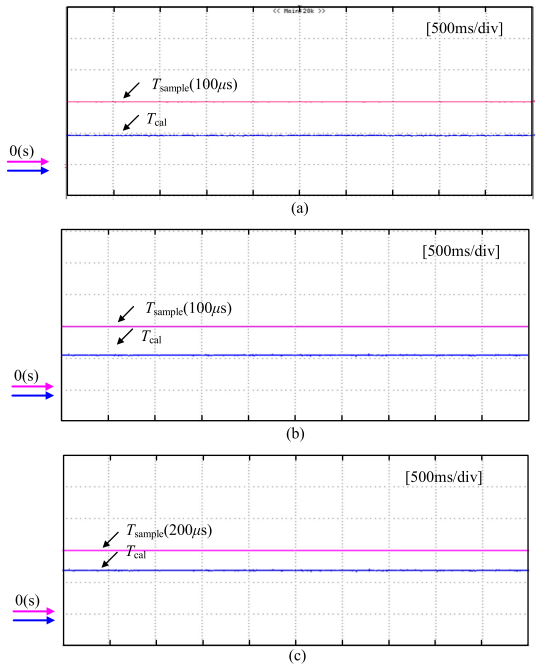

Fig. 13. Calculation time of different methods. (a) Improved three-vector-based model predictive control. (b) Space vector modulation model predictive control. (c) Conventional model predictive control.

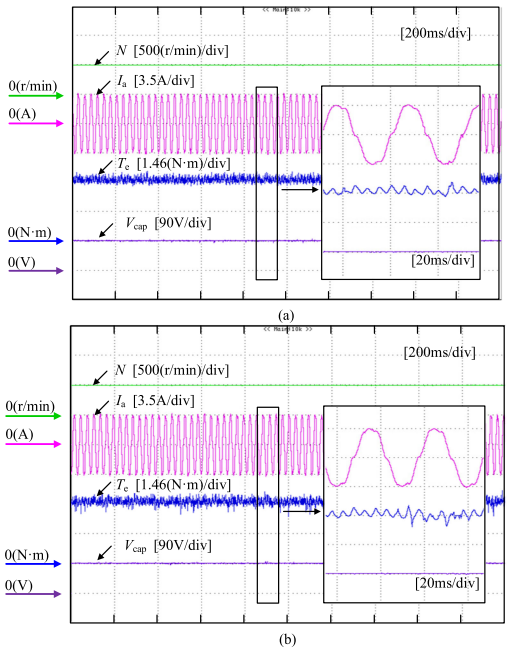

Fig. 14. Control static performance at 500 r/min with the load of 3 N·m with same switching frequency 1.8 kHz. (a) Improved three-vector-based model predictive control. (b) Space vector modulation model predictive control.

either the same sampling frequency or the same switching frequency.

VI. Conclusion

An improved three-vector MPC for the HI-OW-PMSM system has been proposed in this article. First, a new prediction model of dc-link capacitor voltage based on energy storage model has been proposed and thus a novel cost function without weighting factors is obtained. Moreover, a three-vector selection strategy without sector division has been carried out so immediate determination of the three optimal voltage vectors and their duty cycles have been achieved. Accordingly, the control performance has been improved and the system calculation burden has been reduced compared with the C-MPC and SVM-MPC for the HI-OW-PMSM system. Finally, the experimental results have validated the effectiveness and superiority of the proposed method. In addition, the proposed ITMPC has simplified the control procedure and the calculation time of ITMPC is lower than that of C-MPC and SVM-MPC.

References

[1] F. Niu, B. Wang, A. S. Babel, K. Li, and E. G. Strangas, "Comparative evaluation of direct torque control strategies for permanent magnet synchronous machines," *IEEE Trans. Power Electron.*, vol. 31, no. 2, pp. 1408–1424, Feb. 2016.

[2] Z. Zhou, C. Xia, Y. Yan, Z. Wang, and T. Shi, "Torque ripple minimization of predictive torque control for PMSM with extended control set," *IEEE Trans. Ind. Electron.*, vol. 64, no. 9, pp. 6930–6939, Sep. 2017.

[3] S. Hu, Z. Liang, W. Zhang, and X. He, "Research on the integration of hybrid energy storage system and dual three-phase PMSM drive in eV," *IEEE Trans. Ind. Electron.*, vol. 65, no. 8, pp. 6602–6611, Aug. 2018.

[4] T. Kawabata, E. C. Ejiogu, Y. Kawabata, and K. Nishiyama, "New open-winding configurations for high-power inverters," in *Proc. Inst. Ind. Electron.*, 1997, vol. 2, pp. 457–462.

[5] P. Sandulescu, F. Meinguet, X. Kestelyn, E. Semail, and A. Bruyère, "Control strategies for open-end winding drives operating in the flux-weakening region," *IEEE Trans. Power Electron.*, vol. 29, no. 9, pp. 4829–4842, Sep. 2014.

[6] H. Nian and Y. Zhou, "Investigation of open-winding PMSG system with the integration of fully controlled and uncontrolled converter," *IEEE Trans. Ind. Appl.*, vol. 51, no. 1, pp. 429–439, Jan./Feb. 2015.

[7] C. Sun, D. Sun, Z. Zheng, and H. Nian, "Simplified model predictive control for dual inverter-fed open-winding permanent magnet synchronous motor," *IEEE Trans. Energy Convers.*, vol. 33, no. 4, pp. 1846–1854, Dec. 2018.

[8] H. Zhan, Z. Zhu, and M. Odavic, "Analysis and suppression of zero sequence circulating current in open winding PMSM drives with common DC bus," *IEEE Trans. Ind. Appl.*, vol. 53, no. 4, pp. 3609–3620, Jul./Aug. 2017.

[9] Y. Lee and J. Ha, "Hybrid modulation of dual inverter for open-end permanent magnet synchronous motor," *IEEE Trans. Power Electron.*, vol. 30, no. 6, pp. 3286–3299, Jun. 2015.

[10] D. Sun, Z. Zheng, B. Lin, W. Zhou, and M. Chen, "A hybrid PWM-Based field weakening strategy for a hybrid-inverter-driven open-winding PMSM system," *IEEE Trans. Energy Convers.*, vol. 32, no. 3, pp. 857–865, Sep. 2017.

[11] W. Zhou, D. Sun, and B. Lin, "A modified flux weakening direct torque control for open winding PMSM system fed by hybrid inverter," in *Proc. 17th Int. Conf. Elect. Mach. Syst.*, 2014, pp. 2917–2922.

[12] B. Zhu, K. Rajashekara, and H. Kubo, "Comparison between current-based and flux/torque-based model predictive control methods for open-end winding induction motor drives," *IET Elect. Power Appl.*, vol. 11, no. 8, pp. 1397–1406, Sep. 2017.

[13] L. Chen and H. Nian, "Model predictive control of semi-controllable open winding PMSG based on three level NPC converter," in *Proc. 19th Int. Conf. Elect. Mach. Syst.*, 2016, pp. 1–7.

[14] B. Zhu, K. Rajashekara, and H. Kubo, "A novel predictive current control for open-end winding induction motor drive with reduced computation burden and enhanced zero sequence current suppression," in *Proc. Int. Conf. Appl. Power Electron. Conf. Expo.*, 2017, pp. 552–557.

[15] S. Chowdhury, P. W. Wheeler, C. Gerada, and C. Patel, "Model predictive control for a dual-active bridge inverter with a floating bridge," *IEEE Trans. Ind. Electron.*, vol. 63, no. 9, pp. 5558–5568, Sep. 2016.

[16] Y. Zhang, H. Yang, and B. Xia, "Model-Predictive control of induction motor drives: Torque control versus flux control," *IEEE Trans. Ind. Appl.*, vol. 52, no. 5, pp. 4050–4060, Sep./Oct. 2016.

[17] Y. Zhang and H. Yang, "Model-Predictive flux control of induction motor drives with switching instant optimization," *IEEE Trans. Energy Convers.*, vol. 30, no. 3, pp. 1113–1122, Sep. 2015.
[18] L. Guo, X. Zhang, S. Yang, Z. Xie, L. Wang, and R. Cao, "Simplified model predictive direct torque control method without weighting factors for permanent magnet synchronous generator-based wind power system," *IET Elect. Power Appl.*, vol. 11, no. 5, pp. 793–804, 2017.
[19] K. M. R. Eswar, K. V. P. Kumar, and T. V. Kumar, "A simplified predictive torque control scheme for open end winding induction motor drive," *IEEE J. Emerg. Sel. Top. Power Electron,* vol. 7, no. 2, pp. 1162–1172, Jun. 2019.
[20] X. Zhang and K. Wang, "Current prediction based zero sequence current suppression strategy for the Semi-controlled open-winding PMSM generation system with a common DC bus," *IEEE Trans. Ind. Electron.*, vol. 65, no. 8, pp. 6066–6076, Aug. 2018.
[21] Y. Luo and C. Liu, "Model predictive torque control of an open-end winding PMSM with reduced computation time," in *Proc. 20th Int. Conf. Elect. Mach. Syst.*, 2017, pp. 1–6.
[22] K. R. Zhu and H. Kubo, "A novel predictive current control for open-end winding induction motor drive with reduced calculation burden and enhanced zero sequence current suppression," in *Proc. Conf. Appl. Power Electron. Expo.*, 2017, pp. 552–557.
[23] X. Wang and D. Sun, "Three-Vector-Based low-complexity model predictive direct power control strategy for doubly fed induction generators," *IEEE Trans. Power Electron.*, vol. 32, no. 1, pp. 773–782, Jan. 2017.
[24] Y. Zhang, J. Liu, H. Yang, and S. Fan, "New insights into model predictive control for three-phase power converters," *IEEE Trans. Ind. Appl.*, vol. 55, no. 2, pp. 1973–1982, Mar./Apr. 2019.
[25] Y. Zhang, Y. Bai, and H. Yang, "A universal multiple-vector-based model predictive control of induction motor drives," *IEEE Trans. Power Electron.*, vol. 33, no. 8, pp. 6957–6969, Aug. 2018.
[26] Y. Zhang, D. Xu, J. Liu, S. Gao, and W. Xu, "Performance improvement of model-predictive current control of permanent magnet synchronous motor drives," *IEEE Trans. Ind. Appl.*, vol. 53, no. 4, pp. 3683–3695, Jul./Aug. 2017.
[27] W. Xie *et al.*, "Finite-Control-Set model predictive torque control with a deadbeat solution for PMSM drives," *IEEE Trans. Ind. Electron.*, vol. 62, no. 9, pp. 5402–5410, Sep. 2015.
[28] C. Sun, D. Sun, Z. Zheng, and H. Nian, "Simplified model predictive control for dual inverter-fed open-winding permanent magnet synchronous motor," *IEEE Trans. Energy Convers.*, vol. 33, no. 4, pp. 1846–1854, Dec. 2018.

Chong Sun was born in 1993. He received the M.S. degree in electrical engineering from Zhejiang University, Hangzhou, China, in 2019.

He is currently with the Lishui Power Supply Company of State Grid Zhejiang Electric Power Co., Ltd., Hangzhou, China. His current research interests include power electronics and advanced control strategy of electric machine.

Dan Sun (Senior Member, IEEE) received the B.S. from Shenyang Jianzhu University, Shenyang, China, in 1997, the M.S. degree from Hohai University, Nanjing, China, in 2000, and the Ph.D. degree from Zhejiang University, Hangzhou, China, in 2004, all in electrical engineering.

In 2004, she joined the College of Electrical Engineering, Zhejiang University, where she has been a Full Professor since 2017. Her research interests include the advanced electric machine drives and control for renewable energy power generation system.

Wenhan Chen was born in 1996. He received the B.S. degree in electrical engineering in 2018 from Zhejiang University, Hangzhou, China, where he is currently working toward the M.S. degree in electrical engineering.

His current research interests include advanced control strategy of electrical machine drive.

Heng Nian (Senior Member, IEEE) received the B.Eng. and M.Eng. degrees from the HeFei University of Technology, Hefei, China, 1999 and 2002, respectively, and the Ph.D. degree from Zhejiang University, Hangzhou, China, in 2005, all in electrical engineering.

From 2005 to 2007, he was as a Post-doctoral with the College of Electrical Engineering, Zhejiang University. In 2007, he was promoted as an Associate Professor and since 2016, has been a Full Professor with the College of Electrical Engineering, Zhejiang University. From 2013 to 2014, he was a Visiting Scholar with the Department of Electrical, Computer, and System Engineering, Rensselaer Polytechnic Institute, Troy, NY, USA. He has authored or coauthored more than 40 IEEE/IET Transaction papers and holds more than 20 issued/pending patents. His current research interests include the optimal design and operation control for wind power generation system.